

## Article

# Two New Picoline-Derived Meroterpenoids with Anti-Acetylcholinesterase Activity from Ascidian-Derived Fungus *Amphichorda felina*

Minghua Jiang <sup>1,2</sup> , Heng Guo <sup>1,2</sup>, Qilin Wu <sup>1,2</sup>, Siwen Yuan <sup>1,2</sup> and Lan Liu <sup>1,2,3,\*</sup> <sup>1</sup> School of Marine Sciences, Sun Yat-sen University, Zhuhai 519082, China<sup>2</sup> Southern Marine Science and Engineering Guangdong Laboratory (Zhuhai), Zhuhai 519000, China<sup>3</sup> Pearl River Estuary Marine Ecosystem Research Station, Ministry of Education, Zhuhai 519082, China

\* Correspondence: cesllan@mail.sysu.edu.cn

**Abstract:** Amphichoterpenoids D (**1**) and E (**2**), two new picoline-derived meroterpenoids with a rare 6/6/6 tricyclic pyrano[3,2-c]pyridinyl- $\gamma$ -pyranone scaffold, were isolated from the ascidian-derived fungus *Amphichorda felina* SYSU-MS7908. Their structures, including the absolute configurations, were established by extensive spectroscopic methods (1D and 2D NMR and high-resolution mass spectrometry) and ECD calculations. Compounds **1** and **2** showed anti-acetylcholinesterase (anti-AChE) activities with IC<sub>50</sub> values of 12.5  $\mu$ M and 11.6  $\mu$ M, respectively. The binding interactions between **1**, **2**, and AChE were investigated using molecular docking analyses.

**Keywords:** fungal meroterpenoid; picoline; *Amphichorda felina*; anti-acetylcholinesterase activity



**Citation:** Jiang, M.; Guo, H.; Wu, Q.; Yuan, S.; Liu, L. Two New Picoline-Derived Meroterpenoids with Anti-Acetylcholinesterase Activity from Ascidian-Derived Fungus *Amphichorda felina*. *Molecules* **2022**, *27*, 5076. <https://doi.org/10.3390/molecules27165076>

Academic Editor: Akihito Yokosuka

Received: 14 June 2022

Accepted: 8 August 2022

Published: 10 August 2022

**Publisher's Note:** MDPI stays neutral with regard to jurisdictional claims in published maps and institutional affiliations.



**Copyright:** © 2022 by the authors. Licensee MDPI, Basel, Switzerland. This article is an open access article distributed under the terms and conditions of the Creative Commons Attribution (CC BY) license (<https://creativecommons.org/licenses/by/4.0/>).

## 1. Introduction

Meroterpenoids are a class of hybrid secondary metabolites widely distributed in nature, partially derived from a mixed terpenoid biosynthetic pathway [1–4]. Fungi are a promising source of meroterpenoids with chemical structural diversity and potent bioactivities [1,2,4]. Significantly, some fungal meroterpenes have been used as clinical drugs or promising leads, e.g., immunosuppressant drugs: mycophenolic acid [5], antimicrobial and anti-angiogenesis agents: fumagillin [6,7], clinical anticancer drugs: antroquinonol and 4-acetyl antroquinonol B [8], anti-inflammatory berkeleyacetal C [9] and anti-acetylcholinesterase (anti-AChE): territrem B [10].

Owing to their difference in nonterpenoid starting units, fungal meroterpenoids can be divided into the following four classes: polyketide–terpenoids, indole–terpenoids, shikimate–terpenoids, and miscellaneous meroterpenoids [1,3]. Meroterpenoids possessing pyridine units are a particular class of rare discovered natural products [11–16]. Pyridine is a crucial active functional scaffold for many drugs in medicinal chemistry [17]. Thus, these molecules always display rich structural diversity and broad bioactivities (Figure 1), such as cholesterol acyltransferase inhibitor pyripyropenes [11], anti-butyrylcholinesterase terreuspyridine [14], protein tyrosine phosphatase inhibitor penerpene B [13], anti-allergic dysivillosins [15], and anti-AChE amphichoterpenoids [12], which have attracted widespread attention from chemists and biologists to explore their structural diversity, biosynthesis, and bioactivities [11,18–20].

Marine fungi have been widely recognized as the essential source of bioactive natural products [21–25]. Our research group has focused on discovering secondary metabolites from ascidian-derived fungi [26–29]. Recently, we have reported anti-AChE meroterpenoids (amphichoterpenoids) [12], antiplatelet and antithrombotic cyclodepsipeptide [30], and anti-inflammatory polyketones [31] from the ascidian-derived fungus *Amphichorda felina* SYSU-MS7908. Amphichoterpenoids are the first example of picoline-derived meroterpenoids featuring a 6/6/6 tricyclic pyrano[3,2-c]pyridinyl- $\gamma$ -pyranone skeleton, with the picoline

as the nonterpenoid starting moiety [12]. In order to obtain more of this type of molecules, a chemical investigation of the remaining metabolic components of this fungus strain led to the identification of two new picoline-derived meroterpenoids, amphichoterpenoids D and E, (**1** and **2**) (Figure 2). Herein, the details of the isolation, structural elucidation, anti-AChE activity, and molecular docking studies of compounds **1** and **2** are reported.

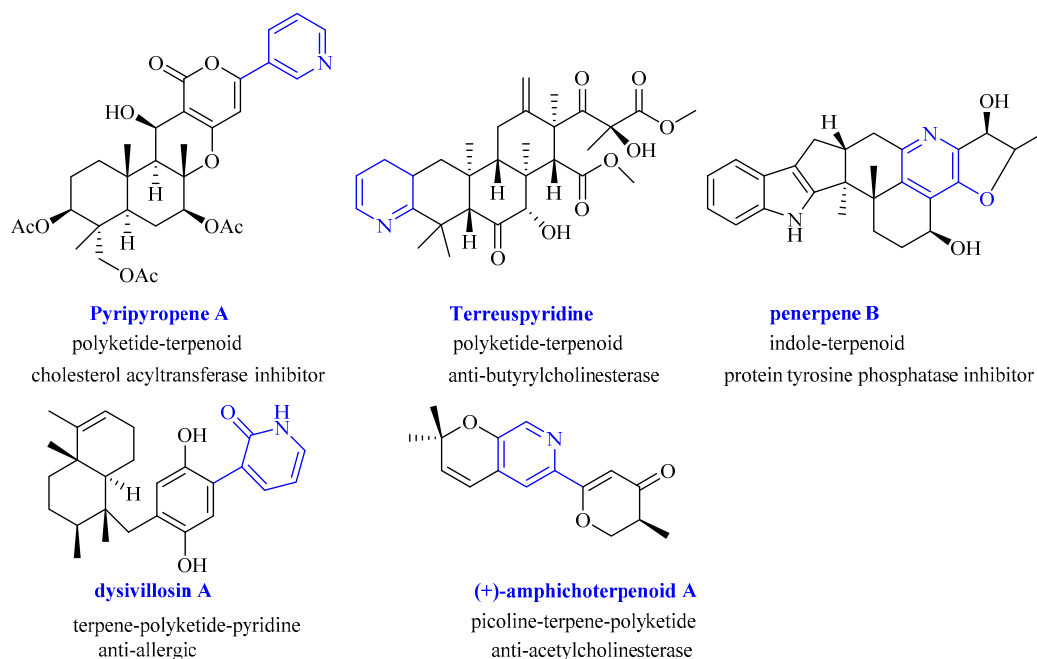


**Figure 1.** Chemical structure and bioactivities of the representative meroterpenoids with pyridine unit.

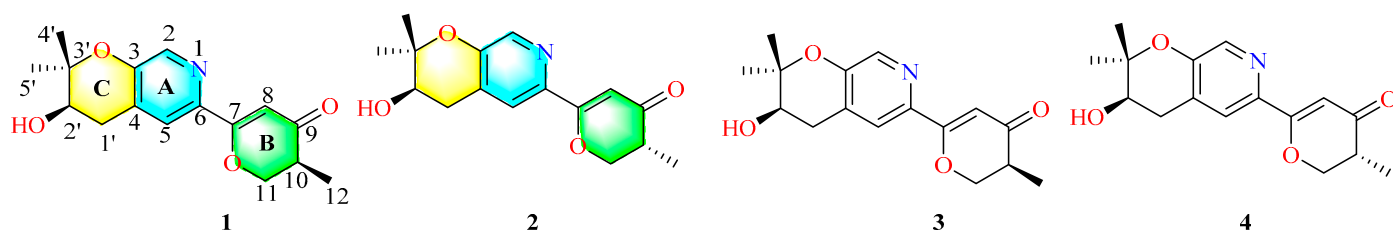


**Figure 2.** Chemical structures of compounds **1–4**.

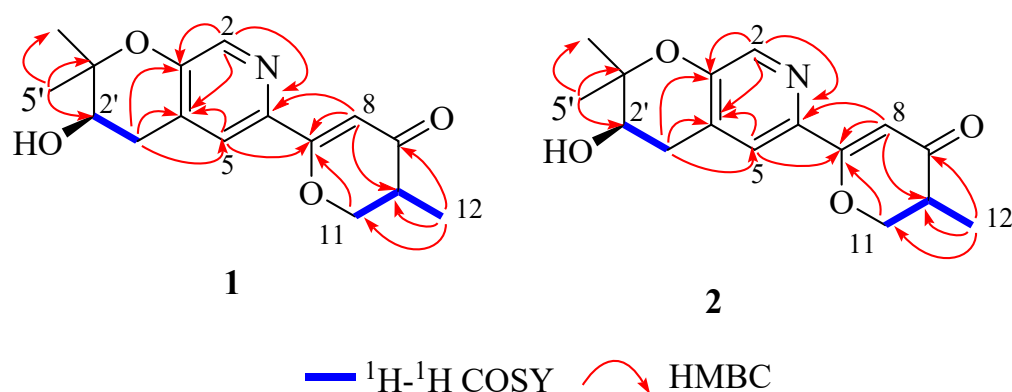
## 2. Results and Discussion

Compound **1** was isolated as a white powder. Its molecular formula was established as  $C_{16}H_{19}NO_4$  by the positive HR-ESI-MS ions at  $m/z$  290.13887  $[M+H]^+$  (calcd for  $C_{16}H_{20}NO_4$ , 290.13868), indicating 8 degrees of unsaturation. The  $^1H$  NMR spectrum (Table 1) displayed two aromatic protons [ $\delta_H$  8.22 (s, H-2); 7.57 (s, H-5)] owing to a 3,4,6-trisubstituted pyridine ring, one olefinic proton [ $\delta_H$  6.40 (s, H-8)], two methines [ $\delta_H$  2.66 (m, H-10); one oxygenated CH  $\delta_H$  3.88 (t, H-2')], two methylenes [ $\delta_H$  4.25 (t,  $J = 10.8$  Hz, H-11a), 4.65 (dd,  $J = 11.1, 5.0$  Hz, H-11b); 2.81 (dd,  $J = 17.4, 4.5$  Hz, H-1'a), 3.08 (dd,  $J = 17.4, 4.5$  Hz, H-1'b)], and three methyls [ $\delta_H$  1.18 (d,  $J = 7.0$  Hz, H-12); 1.36 (s, H-4'); 1.40 (s, H-5')]. The  $^{13}C$  NMR and DEPT spectral data (Table 1) of **1** displayed the presence of 16 carbons, including eight  $sp^3$  and eight  $sp^2$  carbons. Except for five  $sp^2$  carbons ( $\delta_C$  140.3, 152.4, 127.7, 122.7, 142.3) belonging to the pyridine ring (ring A), the remaining three  $sp^2$  carbons were classified as one carbonyl group ( $\delta_C$  196.1) and an olefin group ( $\delta_C$  168.2, 101.6). The 1D NMR data and molecular formula indicated that **1** is an amphichoterpenoid type meroterpenoid with a tricyclic ring system [12].

**Table 1.**  $^1\text{H}$  (400 MHz) and  $^{13}\text{C}$  (100 MHz) NMR data for compounds **1** and **2** ( $\text{CDCl}_3$ ).

No.	<b>1</b>		<b>2</b>	
	$\delta_{\text{C}}$ , Type	$\delta_{\text{H}}$ , Mult (J in Hz)	$\delta_{\text{C}}$ , Type	$\delta_{\text{H}}$ , Mult (J in Hz)
2	140.3, CH	8.22, s	140.3, CH	8.22, s
3	152.4, C		152.4, C	
4	127.7, C		127.6, C	
5	122.7, CH	7.57, s	122.7, CH	7.57, s
6	142.3, C		142.3, C	
7	168.2, C		167.9, C	
8	101.6, CH	6.40, s	101.6, CH	6.40, s
9	196.1, C		196.1, C	
10	39.27, CH	2.66, m	39.27, CH	2.67, m
11	73.68, $\text{CH}_2$	a:4.65, dd (11.1, 5.0); b: 4.25, t (10.8)	73.69, $\text{CH}_2$	a:4.64, dd (11.1, 5.0); b: 4.25, t (10.8)
12	11.34, $\text{CH}_3$	1.18, d (7.0)	11.37, $\text{CH}_3$	1.18, d (7.0)
1'	30.9, $\text{CH}_2$	a: 3.08 dd (17.4, 4.5); b: 2.81 dd (17.4, 4.5)	30.9, $\text{CH}_2$	a: 3.08 dd (17.4, 4.5); b: 2.81 dd (17.4, 4.5)
2'	68.9, CH	3.88, t (9.9)	68.9, CH	3.89, t (9.9)
3'	78.7, C		78.6, C	
4'	25.0, $\text{CH}_3$	1.36, s	25.0, $\text{CH}_3$	1.36, s
5'	22.1, $\text{CH}_3$	1.40, s	22.1, $\text{CH}_3$	1.40, s

Further analyses of the  $^1\text{H}$ - $^1\text{H}$  COSY and HMBC spectra resulted in the identification of the planar structure of **1**. The  $^1\text{H}$ - $^1\text{H}$  COSY spectrum indicated the presence of two independent spin systems,  $\text{H}_2$ -11/ $\text{H}$ -10/ $\text{H}_3$ -12 and  $\text{H}_2$ -1'/ $\text{H}$ -2' (Figure 3). The HMBC cross-peaks from H-2 to C-3, C-4, and C-6, and from H-5 to C-3, and their chemical shifts, can establish the core fragment of the pyridine ring (unit A). Subsequently, the substructure of the  $\gamma$ -pyranone ring (unit B), located at C-6 of unit A, was determined by analyzing the  $^1\text{H}$ - $^1\text{H}$  COSY of  $\text{H}_2$ -11/ $\text{H}$ -10/ $\text{H}_3$ -12, and the key HMBC correlations from H-5 to C-7; from H-8 to C-6, C-7, and C-10; from H-11 to C-7; from  $\text{H}_3$ -12 to C-9, C-10, and C-11 (Figure 3). The  $^1\text{H}$ - $^1\text{H}$  COSY of  $\text{H}_2$ -1'/ $\text{H}$ -2' and the HMBC correlations from  $\text{H}_2$ -1' to C-3, C-4, C-5, C-2', and C-3'; from  $\text{H}_3$ -5' to C-2', C-3' and C-4',  $\text{H}_3$ -4' to C-2', C-3' and C-5' along with the required one degree of unsaturation, revealed a dimethyl-substituted pyran ring (unit C) fused with unit A. Therefore, the resulting planar structure of **1** was established (Figure 3).

**Figure 3.** Key  $^1\text{H}$ - $^1\text{H}$  COSY and HMBC correlations of compounds **1** and **2**.

Compound **2** was obtained as a white solid. The molecular formula was assigned as  $\text{C}_{16}\text{H}_{19}\text{NO}_4$  based on positive-ion HR-ESI-MS ( $m/z$  290.13876  $[\text{M}+\text{H}]^+$  (calcd. for  $\text{C}_{16}\text{H}_{20}\text{NO}_4$ , 290.13868). The detailed analysis of its NMR spectroscopic data (Table 1) revealed that **2** possesses an identical planar structure to **1**, confirmed by the extensive 2D NMR spectroscopic analysis (Figure 3). Based on compounds **1** and **2** purified from the same fraction with different optical rotations, a minor variation ( $\pm 0.03$ ) of  $\delta_{\text{C}}$  (C-10, C-11, and C-12), their NOESY spectrum analysis (Figure S23), and opposite Cotton effects

at 320 nm in their experimental ECD spectra (Figure 4), it is speculated that they were 10-epimers.

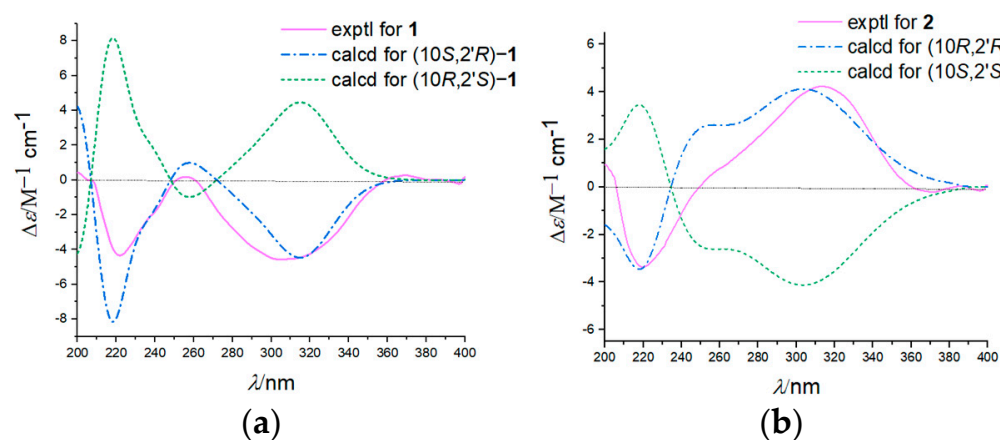


**Figure 4.** Experimental and calculated ECD spectra of compounds **1** (a) and **2** (b).

Compounds **1** and **2** are a pair of epimers exhibiting the same planar structure with only 2 chiral centers at C-10 and C-2', suggesting four possible configurations (10*S*, 2'*R*), (10*R*, 2'*S*), (10*R*, 2'*R*) and (10*S*, 2'*S*). Thus, the absolute configurations were determined by calculating their theoretical ECD and comparing them to the experimental curves and cotton effect values. The theoretical ECD spectrums were constructed by the time-dependent density functional theory (TDDFT) method at the B3LYP/6–311G\*\* level in methanol. The predicted ECD curves of (10*S*, 2'*R*) –**1** and (10*R*, 2'*R*) –**2** were matched well with the experimental ones (Figure 4). Furthermore, the experimental ECD curve of **1** was close to that of (10*S*, 2'*R*) –amphichoterpenoid B previously reported by Jiang M. et al. using X-ray diffraction, which supported the absolute configurations of **1** as 10*S*, 2'*R* (Figure S24) [12]. So, the absolute configurations of **1** and **2** were determined as 10*S*, 2'*R*, and 10*R*, 2'*R*, respectively. Consequently, the structures of **1** and **2** were established, as shown in Figure 2, and were named amphichoterpenoids D and E.

Amphichoterpenoids D (**1**) and E (**2**) are the second report of picoline-derived meroterpenoids with 6/6/6 tricyclic pyrano[3,2-*c*]pyridinyl- $\gamma$ -pyranone scaffold, which may be derived from the lysine-terpenoid-polyketone hybrid biosynthetic pathway [12]. This pair of epimers (**1**, **2**) are the direct biogenic precursors of amphichoterpenoids A–C. This study added members of the rare class of picoline-derived meroterpenoids [12].

The acetylcholinesterase (AChE) inhibitor is the primary drug target for treating Alzheimer's disease [10,32,33]. The huperzine A, physostigmine, berberine, and marketed drugs (galanthamine and rivastigmine) were representative natural products derived-AChE reversible inhibitors with significant activity [34–36]. Here, the AChE inhibitory activities of compounds **1** and **2** were evaluated by Ellman's method and using rivastigmine as the positive control [12,37]. Compounds **1** and **2** exhibited AChE inhibitory activity with  $IC_{50}$  values of 12.5  $\mu\text{M}$  and 11.6  $\mu\text{M}$ , respectively, significantly less active than the positive control, rivastigmine ( $IC_{50}$ , 3.9  $\mu\text{M}$ ). About 38% of the naturally-derived alkaloids (55 molecules) were considered potential AChE inhibitors with an  $IC_{50} \leq 10 \mu\text{M}$  [34,35]. Here, we have added a new class of natural meroterpenoid alkaloids for AChE inhibitors. Besides, because compounds **1**, **2**, and (+)/(–)-amphichoterpenoids A (**3**, **4**) (Figure 2) [12] have the same planar structure but quite different anti-AChE activities in vitro (Table S3), molecular docking analysis was performed to investigate the mechanism of the inhibitory effects of amphichoterpenoids on the AChE enzyme (PDB ID: 1QTI). The results (Figure 5, Table 2) suggested that compounds **1–4** matched well in the protein-binding pocket of AChE protein, but different interactions with AChE were found. Generally, the low binding energy indicates that the active compound is easily bound to the protein. The binding energy of the AChE enzyme and **1** was  $-9.3 \text{ kcal mol}^{-1}$ , with three hydrogen bonds and

two interacting residues, Arg289 and Phe288, which was similar to that of **2** (Figure 4, Table 2). However, the binding affinity between **3** and the AChE enzyme was  $-7.9$  kcal mol $^{-1}$ , with two hydrogen bonds and two interaction residues, Leu305 and Glu306, that was higher than that of **1**, **2**, and lower than that of **4** (binding energy:  $-6.8$  kcal mol $^{-1}$ , without hydrogen bond) (Figure 5, Table 2). It is well known that there are four subsites in the inhibitor-binding gorge-like pocket of AChE, including the catalytic active site (CAS, including Ser200, His440, and Glu327), the peripheral anionic site (PAS, including Tyr70, Tyr121, Trp279, and Asp72), the hydrophobic site (or choline-binding site, including Trp84, Glu199, Phe330, and Tyr442), and the acyl pocket (including Phe288 and Phe290). The binding site between the compounds **1**, **2** and AChE is not CAS but other active sites (Tyr121 and Trp279 residues in the PAS, Phe330 residue in the hydrophobic site, and Phe288 and Phe290 residues in the acyl pocket) that play an important role in the enzyme activity, while compound **3** can interact with some amino acid residues at the substrate binding site (not CAS or PAS) in the pocket of AChE to form hydrogen bonds and hydrophobic interactions, which partially inhibit AChE activity. These results further supported the different acetylcholine inhibitory activities of **1–4** in vitro.

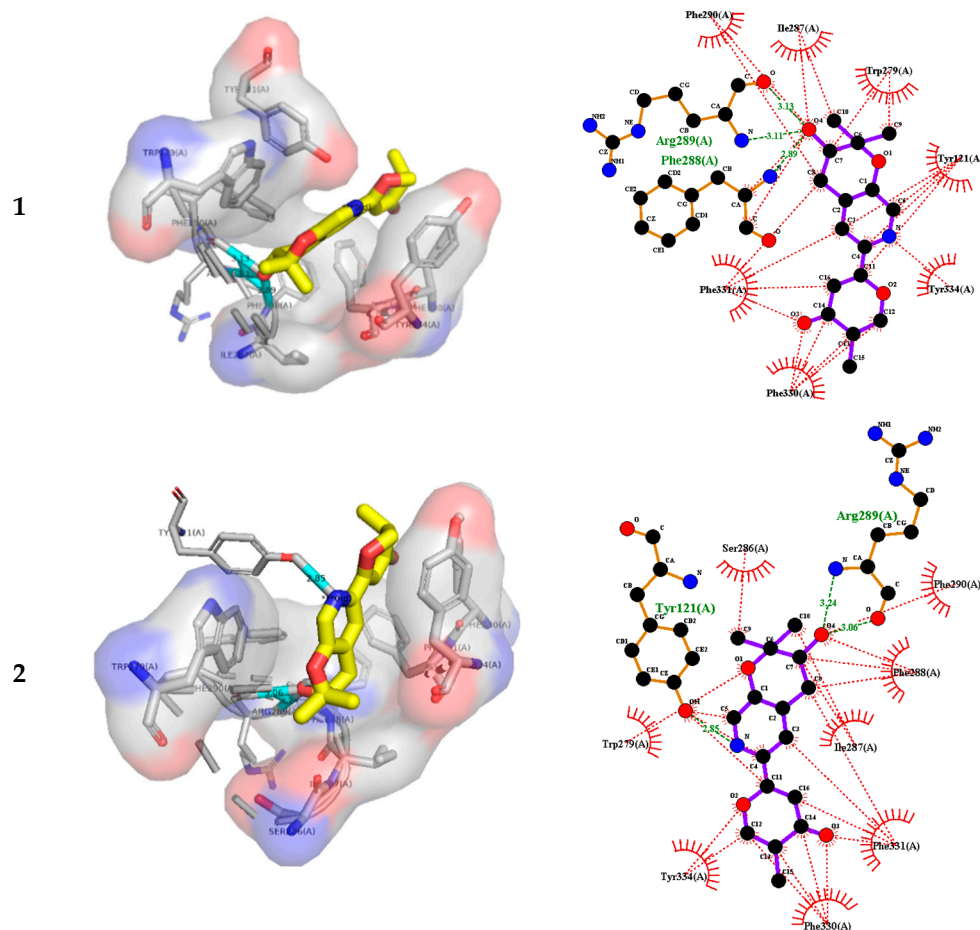
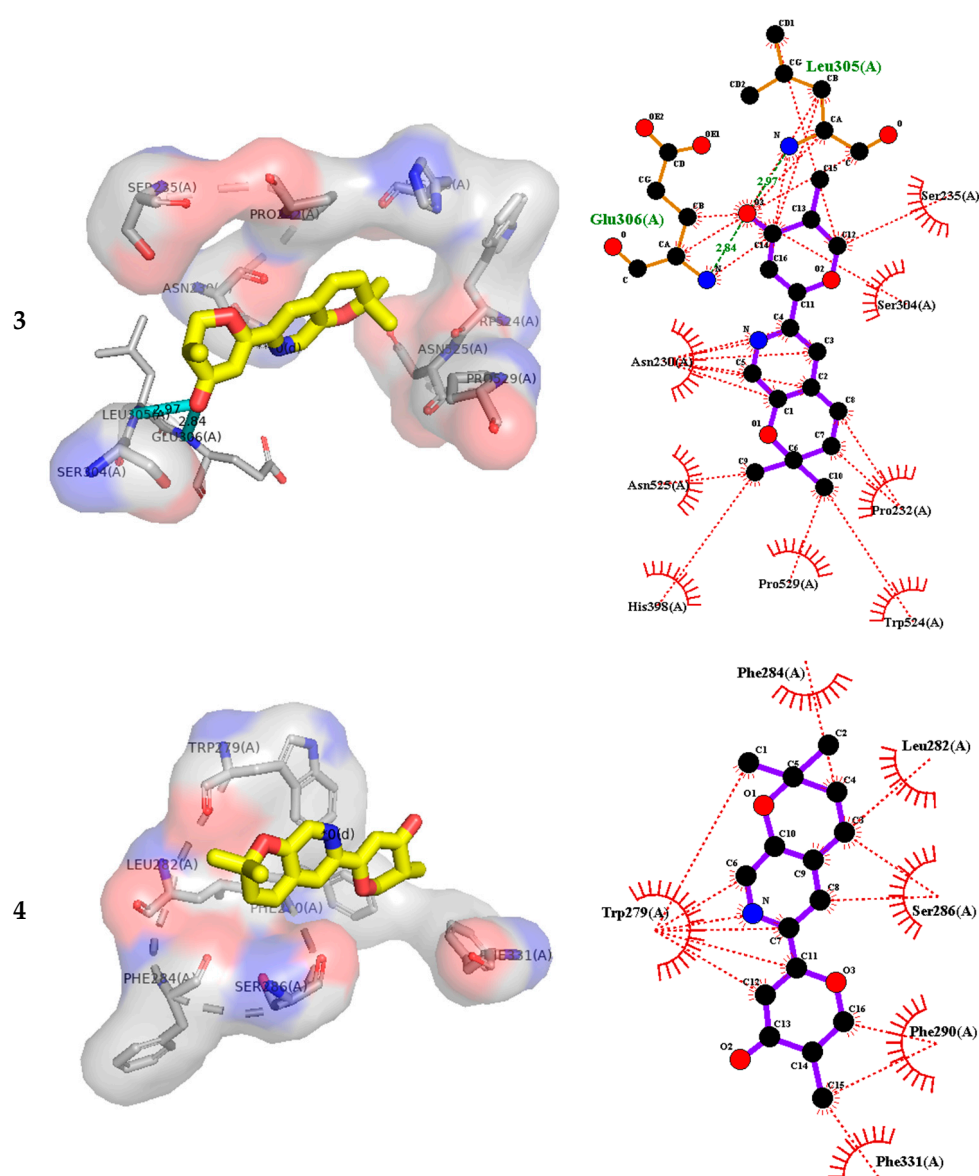


Figure 5. Cont.



**Figure 5.** Docking model for compounds 1–4 with AChE (PDB ID: 1QTI). Hydrogen bonds and hydrophobic interactions are indicated by green and red lines between the atoms involved, respectively.

**Table 2.** Binding energies and targeting residues in the active pocket between compounds 1–4 and AChE (PDB ID: 1QTI).

Compound	log (FBE), kcal/mol	Targeting Residues (H bond Å)	Hydrophobic Interaction Residues
1	−9.3	Arg289(3.13,3.11),Phe288(2.89)	Trp279,Tyr121, Phe330, Phe288,Phe290,Ile287, Tyr334, Phe331
2	−9.3	Arg289(3.24,3.06),Tyr121(2.85)	Trp279,Tyr121, Phe330, Phe288,Phe290,Ile287, Tyr334, Phe331,Ser286
3	−7.9	Leu305(2.97), Glu306(2.84)	Leu305,Glu306,Ser235,Ser304,Pro232,Trp524,Pro529, His398,Asn525,Asn230
4	−6.8	none	Trp279, Phe290,Phe284,Leu282,Ser286, Phe331

### 3. Materials and Methods

#### 3.1. General Experimental Procedures

Optical rotations were carried out on an MCP 200 (Anton Paar, Graz, Austria) polarimeter. UV spectra were measured at a Lambda 950 UV-Vis-NIR spectrophotometer

(PerkinElmer, Akron, OH, USA). A Chirascan-plus Circular Dichroism Spectrometer (Applied Photophysics Ltd., Leatherhead, UK) was used to obtain experimental ECD data. A Fourier transformation infra-red spectrometer (FTIR) coupled with an infra-red microscope EQUINOX 55 (Bruker, Wissembourg, France) recorded the FTIR spectrum. NMR spectra were tested by a BRUKER AVANCE III HD (400 MHz) NMR spectrometer with tetramethylsilane (TMS) as the internal standard. HR-ESIMS data were determined using an Agilent 6530 accurate-Mass Q-TOF LC-MS spectrometer. Column chromatography (CC) was used using silica gel (200–300 mesh, Qingdao Marine Chemical Factory, Qingdao, China). The semi-preparative HPLC was performed on an Essentia LC-16 (Shimadzu, Jiangsu, China). Acetylcholine esterase (AChE) was from Electrophorus electricus (product number: C3389-2KU, Sigma-Aldrich, Saint Louis, MO, USA).

### 3.2. Fungal Material

The strain was identified as *Amphichorda felina* (syn. *Beauveria felina*) SYSU-MS7908 based on the rDNA ITS sequence (GenBank NO. MT786206) [12]. The strain was preserved at Guangdong Microbial Culture Collection Center (GDMCC NO. 61059) and the School of Marine Sciences, Sun Yat-Sen University.

### 3.3. Extraction and Isolation

The strain *A. felina* SYSU-MS7908 was grown on Yeast extract Peptone Dextrose Agar at 26 °C. Then it was cut into pieces and cultivated on rice medium (40 mL rice, 40 mL water with 3% artificial sea salt, and 0.3% peptone) in 200 flasks for 28 days at room temperature. The solid fermented substrate was extracted exhaustively with MeOH three times to obtain a crude extract, then suspended in water and continuously extracted three times with EtOAc. The EtOAc extract (170 g) was fractionated to CC on silica gel (200–300 mesh) and was eluted with petroleum ether/EtOAc of increasing polarity (from 9:1 to 0:10) to obtain six fractions (A–F).

Fr.C was fractionated on a Sephadex LH-20 column with MeOH/CH<sub>2</sub>Cl<sub>2</sub> (1:1) to afford three fractions (Fr.C.1 to Fr.C.3). Fr.C.2 was further fractionated by RP-HPLC (MeOH/H<sub>2</sub>O, 65:35 flow rate 2 mL/min, ACE-C18-AR column 10 × 250 mm, 5 μm) to give subfraction (Fr.C.2.4). Fr.C.2.4 was further purified by RP-HPLC (MeOH/H<sub>2</sub>O, 55:45 flow rate 2 mL/min, ACE-C18-PFP column 10 × 250 mm, 5 μm) to give **1** (3.0 mg) and **2** (2.7 mg).

Amphichoterpenoid D (**1**): White powder; mp 125–128 °C;  $[\alpha]_D^{20}$  −69.8 (*c* 0.20, MeOH); CD (MeOH)  $\lambda_{\max}$  ( $\Delta\epsilon$ ) 220 (−4.10), 318 (−4.15) nm; UV (MeOH)  $\lambda_{\max}$  ( $\log \epsilon$ ) 220 (1.95), 319 (3.24) nm; IR (neat)  $\nu_{\max}$  3359, 2980, 2918, 1643, 1606, 1556, 1376, 1125, 1058, cm<sup>−1</sup>; <sup>1</sup>H NMR (CDCl<sub>3</sub>, 400 MHz) and <sup>13</sup>C NMR (CDCl<sub>3</sub>, 100 MHz) data, see Table 1; HR-ESIMS *m/z* 290.13887 [M+H]<sup>+</sup> (calcd for C<sub>16</sub>H<sub>20</sub>NO<sub>4</sub>, 290.13868).

Amphichoterpenoid E (**2**): White powder; mp 131–134 °C;  $[\alpha]_D^{20}$  +57.6 (*c* 0.20, MeOH); CD (MeOH)  $\lambda_{\max}$  ( $\Delta\epsilon$ ) 220 (−3.92), 320 (+4.21) nm; UV (MeOH)  $\lambda_{\max}$  ( $\log \epsilon$ ) 220 (1.82), 319 (3.25) nm; IR (neat)  $\nu_{\max}$  3359, 2980, 2918, 1643, 1606, 1556, 1376, 1125, 1058, cm<sup>−1</sup>; <sup>1</sup>H NMR (CDCl<sub>3</sub>, 400 MHz) and <sup>13</sup>C NMR (CDCl<sub>3</sub>, 100 MHz) data, see Table 1; HR-ESIMS *m/z* 290.13876 [M+H]<sup>+</sup> (calcd for C<sub>16</sub>H<sub>20</sub>NO<sub>4</sub>, 290.13868).

### 3.4. Calculation of the ECD Spectra

Molecular Merck force field (MMFF) and TDDFT ECD calculations were performed with Spartan'14 software package (Wavefunction Inc., Irvine, CA, USA) and Gaussian 09 program package, respectively, using default grids and convergence criteria. MMFF conformational search generated low-energy conformers within a 10 kcal/mol energy window were subjected to geometry optimization using the DFT method at the B3LYP/6–31 G(d, p) in gas. Frequency calculations were run at the same condition to estimate their relative thermal free energies ( $\Delta G$ ) at 298.15 K. Energies of the low-energy conformers with Boltzmann distribution over 1% in MeOH were re-calculated at the B3LYP/6–311G\*\* level. Solvent effects were taken into account by using an IEF-PCM model. The TDDFT calculations were performed in MeOH using the B3LYP/6–311G\*\* level for all conformers. Rotatory

strengths for a total of 20–50 excited states were calculated. The ECD spectra were produced by the programs SpecDis 1.6 (University of Würzburg, Würzburg, Germany) and OriginPro 8.5 (OriginLab, Ltd., Northampton, MA, USA) using a Gaussian band shape from dipole-length dipolar and rotational strengths with 0.30 eV exponential half-width. The equilibrium population of every conformer at 298.15 K was calculated from its relative free energies using Boltzmann statistics. The calculated spectra of **1** and **2** were generated from the low-energy conformers according to the Boltzmann distribution of each conformer in the MeOH solution. All calculations were performed by Tianhe-2 in National Super Computer Center in Guangzhou.

### 3.5. Anti-Acetylcholinesterase Activity

The acetylcholinesterase (AChE) inhibitory activity of compounds **1** and **2** was evaluated by the modified Ellman's method with rivastigmine as a positive control [12,37]. All experiments were performed in triplicate. The detailed experiment was shown in supporting information.

### 3.6. Molecular Docking

The binding interaction between compounds **1–4** and AChE enzyme at the active site was investigated by molecular docking. Their 3D structures were optimized to establish the lowest energy state and saved in mol.2 file format by chem3D 16.0 software. The protein crystallographic structure of the AChE (PDB ID: 1QTI) was selected from the RCSB Protein Data Bank with 2.5 Å resolution [38]. Molecular docking was conducted using Autodocktools-1.5.6 and PyMOL-2.3.4. Autodock Vina-1.2 [39] was used to study the interaction. PyMOL-2.3.4 and LigPlot + were applied to analyze the result of the binding mode.

## 4. Conclusions

The chemical investigation of the ascidian-derived fungus *A. felina* SYSU-MS7908 afforded a pair of new picoline-derived meroterpenoid epimers, amphichoterpenoids D (**1**) and E (**2**), which possess a 6/6/6 tricyclic pyrano[3,2-c]pyridinyl- $\gamma$ -pyranone scaffold. This study enriched the members of the following rare class of picoline-derived meroterpenoid: amphichoterpenoids. Moreover, **1** and **2** showed potential AChE inhibitory activity, indicating its potential use in the treatment of Alzheimer's disease.

**Supplementary Materials:** The following supporting information can be downloaded at: <https://www.mdpi.com/article/10.3390/molecules27165076/s1>, Figure S1: The HRESIMS spectrum of compound **1**, Figures S2–S8: The 1D and 2D NMR (400 MHz) spectra of compound **1** in CDCl<sub>3</sub>, Figures S9 and S10: The IR/UV spectrum of compound **1**, Figure S11: The HRESIMS spectrum of compound **2**, Figures S12–S18: The 1D and 2D NMR (400 MHz) spectra of compound **2** in CDCl<sub>3</sub>, Figures S19 and S20: The IR/UV spectrum of compound **2**. Figures S21 and S22 and Tables S1 and S2: The energy analysis and low-energy conformers of compounds **1** and **2**. Figure S23: Key NOE correlations of compounds **1** and **2**; Figure S24: The X-ray Single crystal structure of amphichoterpenoid B (**5**) and its ECD spectra. Table S3: Inhibitory activity of compounds **1–5** on AChE.

**Author Contributions:** Conceptualization, L.L.; methodology, L.L. and M.J.; validation, M.J., H.G., Q.W. and S.Y.; formal analysis, H.G. and Q.W.; resources, L.L.; data curation, Q.W.; writing—original draft preparation, M.J. and L.L.; writing—review and editing, M.J.; project administration, M.J.; funding acquisition, L.L. All authors have read and agreed to the published version of the manuscript.

**Funding:** This work was supported by the Key-Area Research and Development Program of Guangdong Province (Grant No. 2020B1111030005), the National Natural Science Foundation of China (Grant No. U20A2001, 41806155), Promoting High-quality Economic Development Special Fund of Guangdong Province (GDNRC[2022]35), Southern Marine Science and Engineering Guangdong Laboratory (Zhuhai) (No. SML2021SP319), the Fundamental Research Funds for the Natural Science Foundation of Guangdong Province (Grant No. 2018A030310304).

**Institutional Review Board Statement:** Not applicable.

**Informed Consent Statement:** Not applicable.

**Data Availability Statement:** Not applicable.

**Acknowledgments:** We acknowledge Shanyue Guan, Yang Li, and Ling Fang of Test Center, Sun Yat-sen University, for helping us to finish the spectra test.

**Conflicts of Interest:** The authors declare no conflict of interest.

**Sample Availability:** Samples of the compounds 1 and 2 are available from the authors.

## References

1. Jiang, M.; Wu, Z.; Liu, L.; Chen, S. The chemistry and biology of fungal meroterpenoids (2009–2019). *Org. Biomol. Chem.* **2021**, *19*, 1644–1704. [[CrossRef](#)] [[PubMed](#)]
2. Geris, R.; Simpson, T.J. Meroterpenoids produced by fungi. *Nat. Prod. Rep.* **2009**, *26*, 1063–1094. [[CrossRef](#)] [[PubMed](#)]
3. Matsuda, Y.; Abe, I. Biosynthesis of fungal meroterpenoids. *Nat. Prod. Rep.* **2016**, *33*, 26–53. [[CrossRef](#)] [[PubMed](#)]
4. Matsuda, Y.; Abe, I. Fungal Meroterpenoids. In *Comprehensive Natural Products III: Chemistry and Biology*; Elsevier: Amsterdam, The Netherlands, 2019; Volume 1, pp. 445–478.
5. Sintchak, M.D.; Fleming, M.A.; Futer, O.; Raybuck, S.A.; Chambers, S.P.; Caron, P.R.; Murcko, M.A.; Wilson, K.P. Structure and mechanism of inosine monophosphate dehydrogenase in complex with the immunosuppressant mycophenolic acid. *Cell* **1996**, *85*, 921–930. [[CrossRef](#)]
6. Liu, S.; Widom, J.; Kemp, C.W.; Crews, C.M.; Clardy, J. Structure of human methionine aminopeptidase-2 complexed with fumagillin. *Science* **1998**, *282*, 1324–1327. [[CrossRef](#)]
7. Molina, J.M.; Tourneur, M.; Sarfati, C.; Chevret, S.; de Gouvello, A.; Gobert, J.G.; Balkan, S.; Derouin, F.; Agence Natl Recherches, SIDA 090 St. Fumagillin treatment of intestinal microsporidiosis. *N. Engl. J. Med.* **2002**, *346*, 1963–1969. [[CrossRef](#)]
8. Chen, M.C.; Cho, T.Y.; Kuo, Y.H.; Lee, T.H. Meroterpenoids from a Medicinal Fungus *Antrodia cinnamomea*. *J. Nat. Prod.* **2017**, *80*, 2439–2446. [[CrossRef](#)]
9. Stierle, D.B.; Stierle, A.A.; Patacini, B. The berkeleyacetals, three meroterpenes from a deep water acid mine waste *Penicillium*. *J. Nat. Prod.* **2007**, *70*, 1820–1823. [[CrossRef](#)]
10. Peng, F.C. Acetylcholinesterase Inhibition by Territrem-B Derivatives. *J. Nat. Prod.* **1995**, *58*, 857–862. [[CrossRef](#)]
11. Itoh, T.; Tokunaga, K.; Matsuda, Y.; Fujii, I.; Abe, I.; Ebizuka, Y.; Kushiro, T. Reconstitution of a fungal meroterpenoid biosynthesis reveals the involvement of a novel family of terpene cyclases. *Nat. Chem.* **2010**, *2*, 858–864. [[CrossRef](#)]
12. Jiang, M.; Wu, Z.; Wu, Q.; Yin, H.; Guo, H.; Yuan, S.; Liu, Z.; Chen, S.; Liu, L. Amphichoterpenoids A–C, unprecedented picoline-derived meroterpenoids from the ascidian-derived fungus *Amphichorda felina* SYSU-MS7908. *Chin. Chem. Lett.* **2021**, *32*, 1893–1896. [[CrossRef](#)]
13. Kong, F.D.; Fan, P.; Zhou, L.M.; Ma, Q.Y.; Xie, Q.Y.; Zheng, H.Z.; Zheng, Z.H.; Zhang, R.S.; Yuan, J.Z.; Dai, H.F.; et al. Peneperpenes A–D, Four Indole Terpenoids with Potent Protein Tyrosine Phosphatase Inhibitory Activity from the Marine-Derived Fungus *Penicillium* sp. KFD28. *Org. Lett.* **2019**, *21*, 4864–4867. [[CrossRef](#)] [[PubMed](#)]
14. Li, H.; Feng, W.; Li, X.; Kang, X.; Yan, S.; Chao, M.; Mo, S.; Sun, W.; Lu, Y.; Chen, C.; et al. Terreuspyridine: An Unexpected Pyridine-Fused Meroterpenoid Alkaloid with a Tetracyclic 6/6/6/6 Skeleton from *Aspergillus terreus*. *Org. Lett.* **2020**, *22*, 7041–7046. [[CrossRef](#)] [[PubMed](#)]
15. Jiao, W.H.; Cheng, B.H.; Shi, G.H.; Chen, G.D.; Gu, B.B.; Zhou, Y.J.; Hong, L.L.; Yang, F.; Liu, Z.Q.; Qiu, S.Q.; et al. Dysivillosins A–D, Unusual Anti-allergic Meroterpenoids from the Marine Sponge *Dysidea villosa*. *Sci. Rep.* **2017**, *7*, 8947–8956. [[CrossRef](#)] [[PubMed](#)]
16. Zhu, L.J.; Hou, Y.L.; Shen, X.Y.; Pan, X.D.; Zhang, X.; Yao, X.S. Monoterpene pyridine alkaloids and phenolics from *Scrophularia ningpoensis* and their cardioprotective effect. *Fitoterapia* **2013**, *88*, 44–49. [[CrossRef](#)]
17. Vitaku, E.; Smith, D.T.; Njardarson, J.T. Analysis of the Structural Diversity, Substitution Patterns, and Frequency of Nitrogen Heterocycles among US FDA Approved Pharmaceuticals. *J. Med. Chem.* **2014**, *57*, 10257–10274. [[CrossRef](#)]
18. Lin, S.X.; Curtis, M.A.; Sperry, J. Pyridine alkaloids with activity in the central nervous system. *Bioorg. Med. Chem.* **2020**, *28*, 115820–115841. [[CrossRef](#)]
19. Yan, Y.J.; Ma, Y.T.; Yang, J.; Horsman, G.P.; Luo, D.; Ji, X.; Huang, S.X. Tropolone Ring Construction in the Biosynthesis of Rubrolone B, a Cationic Tropolone Alkaloid from Endophytic *Streptomyces*. *Org. Lett.* **2016**, *18*, 1254–1257. [[CrossRef](#)]
20. Luo, F.; Hong, S.; Chen, B.; Yin, Y.; Tang, G.; Hu, F.; Zhang, H.; Wang, C. Unveiling of Swainsonine Biosynthesis via a Multibranching Pathway in Fungi. *ACS Chem. Biol.* **2020**, *15*, 2476–2484. [[CrossRef](#)]
21. Jiang, M.; Wu, Z.; Guo, H.; Liu, L.; Chen, S. A Review of Terpenes from Marine-Derived Fungi: 2015–2019. *Mar. Drugs* **2020**, *18*, 321. [[CrossRef](#)]
22. Jiang, M.; Chen, S.; Li, J.; Liu, L. The biological and chemical diversity of tetramic acid compounds from marine-derived microorganisms. *Mar. Drugs* **2020**, *18*, 114. [[CrossRef](#)]

23. Carroll, A.R.; Copp, B.R.; Davis, R.A.; Keyzers, R.A.; Prinsep, M.R. Marine natural products. *Nat. Prod. Rep.* **2022**, *39*, 1122–1171. [[CrossRef](#)]
24. Carroll, A.R.; Copp, B.R.; Davis, R.A.; Keyzers, R.A.; Prinsep, M.R. Marine natural products. *Nat. Prod. Rep.* **2021**, *38*, 362–413. [[CrossRef](#)]
25. Chen, S.; Shen, H.; Deng, Y.; Guo, H.; Jiang, M.; Wu, Z.; Yin, H.; Liu, L. Roussoelins A and B: Two phenols with antioxidant capacity from ascidian-derived fungus *Roussoella siamensis* SYSU-MS4723. *Mar. Life Sci. Technol.* **2020**, *3*, 69–76. [[CrossRef](#)]
26. Niaz, S.I.; Zhang, P.; Shen, H.; Li, J.; Chen, B.; Chen, S.; Liu, L.; He, J. Two new isochromane derivatives penisochromanes A and B from ascidian-derived fungus *Penicillium* sp. 4829. *Nat. Prod. Res.* **2019**, *33*, 1262–1268. [[CrossRef](#)]
27. Chen, S.; Jiang, M.; Chen, B.; Salaenoi, J.; Niaz, S.I.; He, J.; Liu, L. Penicamide A, a unique *N,N'*-ketal quinazolinone alkaloid from ascidian-derived fungus *Penicillium* sp. 4829. *Mar. Drugs* **2019**, *17*, 522. [[CrossRef](#)]
28. Chen, S.; Shen, H.; Zhang, P.; Cheng, H.; Dai, X.; Liu, L. Anti-glioma trichobamide A with an unprecedented tetrahydro-5H-furo [2,3-b]pyrrol-5-one functionality from ascidian-derived fungus *Trichobotrys effusa* 4729. *Chem. Commun.* **2019**, *55*, 1438–1441. [[CrossRef](#)]
29. Chen, S.; Guo, H.; Jiang, M.; Wu, Q.; Li, J.; Shen, H.; Liu, L. Mono- and dimeric xanthenes with anti-glioma and anti-inflammatory activities from the ascidian-derived fungus *Diaporthe* sp. SYSU-MS4722. *Mar. Drugs* **2022**, *20*, 51. [[CrossRef](#)]
30. Pan, N.; Li, Z.C.; Li, Z.H.; Chen, S.H.; Jiang, M.H.; Yang, H.Y.; Liu, Y.S.; Hu, R.; Zeng, Y.W.; Dai, L.H.; et al. Antiplatelet and antithrombotic effects of isaridin E isolated from the marine-derived fungus via downregulating the PI3K/Akt signaling pathway. *Mar. Drugs* **2022**, *20*, 23. [[CrossRef](#)]
31. Yuan, S.; Chen, L.; Wu, Q.; Jiang, M.; Guo, H.; Hu, Z.; Chen, S.; Liu, L.; Gao, Z. Genome Mining of  $\alpha$ -Pyrone Natural Products from Ascidian-Derived Fungus *Amphichorda felina* SYSU-MS7908. *Mar. Drugs* **2022**, *20*, 298. [[CrossRef](#)]
32. Zaki, A.G.; El-Sayed, E.R.; Abd Elkodous, M.; El-Sayyad, G.S. Microbial acetylcholinesterase inhibitors for Alzheimer's therapy: Recent trends on extraction, detection, irradiation-assisted production improvement and nano-structured drug delivery. *Appl. Microbiol. Biotechnol.* **2020**, *104*, 4717–4735. [[CrossRef](#)]
33. Houghton, P.J.; Ren, Y.; Howes, M.J. Acetylcholinesterase inhibitors from plants and fungi. *Nat. Prod. Rep.* **2006**, *23*, 181–199. [[CrossRef](#)]
34. Berkov, S.; Atanasova, M.; Georgiev, B.; Bastida, J.; Doytchinova, I. The Amaryllidaceae alkaloids: An untapped source of acetylcholinesterase inhibitors. *Phytochem. Rev.* **2021**. [[CrossRef](#)]
35. Kong, Y.R.; Tay, K.C.; Su, Y.X.; Wong, C.K.; Tan, W.N.; Khaw, K.Y. Potential of Naturally Derived Alkaloids as Multi-Targeted Therapeutic Agents for Neurodegenerative Diseases. *Molecules* **2021**, *26*, 728. [[CrossRef](#)]
36. Tamfu, A.N.; Kucukaydin, S.; Yeskalyeva, B.; Ozturk, M.; Dinica, R.M. Non-Alkaloid Cholinesterase Inhibitory Compounds from Natural Sources. *Molecules* **2021**, *26*, 5582. [[CrossRef](#)]
37. Ellman, G.L.; Courtney, K.D.; Andres, V., Jr.; Feather-Stone, R.M. A new and rapid colorimetric determination of acetylcholinesterase activity. *Biochem. Pharmacol.* **1961**, *7*, 88–95. [[CrossRef](#)]
38. Bartolucci, C.; Perola, E.; Pilger, C.; Fels, G.; Lamba, D. Three-dimensional structure of a complex of galanthamine (Nivalin (R)) with acetylcholinesterase from *Torpedo californica*: Implications for the design of new anti-Alzheimer drugs. *Proteins* **2001**, *42*, 182–191. [[CrossRef](#)]
39. Eberhardt, J.; Santos-Martins, D.; Tillack, A.F.; Forli, S. AutoDock Vina 1.2.0: New Docking Methods, Expanded Force Field, and Python Bindings. *J. Chem. Inf. Model.* **2021**, *61*, 3891–3898. [[CrossRef](#)]